







Article

Application of Biogenic TiO₂ Nanoparticles as ORR Catalysts on Cathode for Enhanced Performance of Microbial Fuel Cell

Ankit Kumar ^{1,†}, Tabassum Siddiqui ^{2,†}, Soumya Pandit ^{1,*,†} , Arpita Roy ³ , Amel Gacem ⁴ , Abdullah Al Souwaileh ⁵, Abhilasha Singh Mathuriya ⁶, Tasneem Fatma ^{2,*}, Promila Sharma ⁷, Sarvesh Rustagi ⁸, Krishna Kumar Yadav ^{9,10} , Byong-Hun Jeon ^{11,*}  and Hyun-Kyung Park ¹² 

- ¹ Department of Life Sciences, School of Basic Sciences and Research, Sharda University, Greater Noida 201306, India; kankit097@gmail.com
- ² Department of Biosciences, Faculty of Natural Sciences, Jamia Millia Islamia, New Delhi 110025, India; tabassum169253@st.jmi.ac.in
- ³ Department of Biotechnology, Sharda School of Engineering and Technology, Sharda University, Greater Noida 201306, India; arbt2014@gmail.com
- ⁴ Department of Physics, Faculty of Sciences, University 20 Août 1955, Skikda 21000, Algeria; gacem_amel@yahoo.fr
- ⁵ Department of Chemistry, College of Science, King Saud University, Riyadh 11451, Saudi Arabia; souwaileh@gmail.com
- ⁶ Ministry of Environment, Forest and Climate Change, Indira Paryavaran Bhawan, New Delhi 110003, India; imabhilasha@gmail.com
- ⁷ Department of Biotechnology, Graphic Era Deemed to be University, Dehradun 248002, India; promilasharma.bt@geu.ac.in
- ⁸ Department of Food Technology, College of Applied and Life Sciences, Uttaranchal University, Dehradun 248007, India; sarveshrustagi@gmail.com
- ⁹ Faculty of Science and Technology, Madhyanchal Professional University, Bhopal 462044, India; envirokrishna@gmail.com
- ¹⁰ Environmental and Atmospheric Sciences Research Group, Scientific Research Center, Al-Ayen University, Thi-Qar, Nasiriyah 64001, Iraq
- ¹¹ Department of Earth Resources and Environmental Engineering, Hanyang University, 222 Wangsimni-ro, Seongdong-gu, Seoul 04763, Republic of Korea
- ¹² Department of Pediatrics, Hanyang University College of Medicine, 222 Wangsimni-ro, Seongdong-gu, Seoul 04763, Republic of Korea; neopark@hanyang.ac.kr
- * Correspondence: sounip@gmail.com (S.P.); tfatima@jmi.ac.in (T.F.); bhjeon@hanyang.ac.kr (B.-H.J.)
- † These authors contributed equally to this work.



Citation: Kumar, A.; Siddiqui, T.; Pandit, S.; Roy, A.; Gacem, A.; Souwaileh, A.A.; Mathuriya, A.S.; Fatma, T.; Sharma, P.; Rustagi, S.; et al. Application of Biogenic TiO₂ Nanoparticles as ORR Catalysts on Cathode for Enhanced Performance of Microbial Fuel Cell. *Catalysts* **2023**, *13*, 937. <https://doi.org/10.3390/catal13060937>

Academic Editor: Yat Li

Received: 9 May 2023

Revised: 19 May 2023

Accepted: 20 May 2023

Published: 26 May 2023



Copyright: © 2023 by the authors. Licensee MDPI, Basel, Switzerland. This article is an open access article distributed under the terms and conditions of the Creative Commons Attribution (CC BY) license (<https://creativecommons.org/licenses/by/4.0/>).

Abstract: Microbial fuel cells (MFCs) use microorganisms to break down organic matter and generate power, which is an exciting new field of research. MFCs' power generation relies on oxygen reduction (ORR) at the cathode. However, the slow kinetics of the ORR can severely limit the performance of MFCs. Additionally, the growth of biofilm on the cathode hampers the ORR process. In order to ensure the sustainability of MFCs over time, it is crucial to employ bifunctional catalysts that can address these issues. Biogenic titanium dioxide (TiO₂) nanoparticles (NPs) were synthesized and applied to a graphite sheet cathode in this study. Cyanobacteria, *Phormidium* species NCCU-104, was used to bio-fabricate titanium dioxide (TiO₂) nanoparticles. NPs were characterized using SEM and TEM analysis to determine their size, shape, surface morphology, and XRD. The particles had an average size of 18.11 nm, were spherical, and were well-dispersed, according to the results of the physicochemical characterization. TiO₂ NPs were evaluated in MFC using different concentrations (0.5–2.5 mg/cm²) in the cathode to generate electricity and coulombic efficiency. MFC with a cathode impregnated with 2.0 mg/cm² TiO₂ NP produced maximum power density (15.2 W/m³), which was 38% more than 0.5 mg/cm² TiO₂ NP. The overall study results indicated that biogenic TiO₂ nanoparticles (NPs) could be an effective and low-cost catalyst in the oxygen reduction reaction (ORR) and significantly improve biofouling. Due to its efficient and affordable contribution to the ORR, these results imply that biogenic TiO₂ NPs might be a feasible alternative for improving the performance of MFCs.

Keywords: microbial fuel cell; electricity generation; ORR; biogenic titanium dioxide; biofouling; power density; cathode catalyst

1. Introduction

A significant energy deficit and environmental damage result from the unjustified exploitation and utilization of conventional fossil fuels. In order to address these challenges, there has been growing interest in microbial fuel cells (MFCs) as a renewable energy source and a means of treating wastewater. MFCs have the potential to contribute to sustainable development by generating power while simultaneously degrading organic pollutants using electroactive bacteria as biocatalysts [1]. However, the industrial applications of MFCs remain limited [2]. One of the challenges facing MFCs is the restriction posed by cathode catalysts and the difficulty of increasing the MFC reactor volume [3]. The traditional ORR catalyst, the expensive and rare precious metal platinum, can deactivate in polluted environments, making it unsuitable for MFC applications [4]. Due to their high activity and stability, alternative cathode catalysts include carbon matrix composites, transition metals and their oxides, and materials generated from biomass [5]. Among these alternatives, M-N-C catalysts (M = Transition metals Mn, Fe, Ni, Co, etc.) have been identified as promising because they are more stable and have ORR activity [5]. However, incorporating M-N-C catalysts into the cathode of MFCs remains technically challenging, which increases the overall cost [6]. Multiple types of research have been conducted to develop a catalyst that would decrease the overall cost and be sustainable [7,8]. For example, Yin et al. worked on developing ternary nanocomposite MXene@Au@CdS, which can produce excellent photocatalytic hydrogen [9]. Another example is the preparation of perovskite oxides, which have emerged as a broad family of functional materials with promising promise for accelerating the oxygen reduction reaction (ORR), oxygen evolution reaction (OER), hydrogen evolution reaction (HER), and fuel oxidation [10]. Moreover, dopant engineering has been widely used to increase NPGM-based single-atom catalysts (SACs) catalytic activity. However, the coordination environment of the dopant that greatly impacts the electronic configuration of SACs and their electrocatalytic performance has been largely ignored [11].

Titanium is frequently utilized as an antibacterial agent in various industries [12]. It is widely recognized and accepted that Ti releases a limited number of silver ions into a liquid environment, where sulfhydryl group enzymes involved in aerobic bacterial respiration, such as NADH dehydrogenase II, can interact with Ti, which is considered a crucial respiratory site in the respiratory system [13]. TiO₂ nanoparticles have received attention due to their intriguing capabilities and unique structure across a wide range of disciplines [14]. TiO₂ nanoparticles are highly sought after for their numerous exceptional properties, including their chemical stability, low cytotoxicity, favorable biocompatibility, strong light-harvesting abilities, and exceptional photo-induced electron transfer. These properties make TiO₂ nanoparticles a promising material for various applications such as biosensors, bioimaging, and electronic devices [15].

Chemical composition, elemental valence, crystal structure, and surface state all impact ORR. Additionally, the ORR activities are affected by the surface oxygen molecule's adsorption configuration and the associated strength of oxygen binding. High-energy facets expose defective titanium dioxide single crystals for effective oxygen reduction. In this work, the single-crystalline structure, the exposed high-energy facet, and the Ti multiple valences induced by the faulty oxygen vacancies may be strongly connected with the improved ORR activity on the defective TiO₂ [16]. First, the continuous and ordered inner structure and the improved crystallinity should significantly increase electric conductivity and favor quick electron transfer (higher charge mobility), which would lessen electrode polarization in ORR. In TiO₂, the missing oxygen atom from the bulk or surface is taken by one or two "free" electrons in the defective crystal, and the three closest Ti atoms tend

to relax away from the vacancy to strengthen their bonds with the other members of the lattice. In principle, because of the close connection between the adsorbate and the surface, the dissociated adsorption of O₂ on the defective oxygen vacancy might lead to a more effective electron-transfer process and increased ORR kinetics, which are directly connected to the total catalytic performance [16]. Biogenic nanomaterials have an advantage due to their eco-friendly, inexpensive process over chemically synthesized nanomaterials [17]; however, not much report is available on the utilization of biogenic TiO₂ as a cathode catalyst in MFC.

This study used Cyanobacteria, known as Phormidium NCCU-104, to fabricate titanium dioxide (TiO₂) nanoparticles (TiO₂ NPs). By using SEM, TEM and XRD studies, the nanoparticles' physicochemical properties were evaluated. The electrochemical performance of these particles was tested in MFCs by impregnating the cathode with different concentrations of biogenic TiO₂ (0.5–2.5 mg/cm²). Furthermore, the effect of the concentration of the TiO₂NPs as antifouling substances were evaluated on the cathode surface.

2. Results and Discussion

2.1. Synthesis of TiO₂ Nanoparticle

Biogenic synthesis of TiO₂NP was achieved using the aqueous extract of the dry biomass of the Phormidium species. A light green-colored reaction mixture indicated the possible synthesis of nanoparticles. This is consistent with the findings of other studies, such as Santhoshkumar et al. (2014), who used the aqueous extract of *Psidium guajava* to synthesize biogenic TiO₂NP [18]. The cyanobacteria biomass was harvested on the 16th day when the maximum yield was observed. The reaction parameters were optimized using UV-Vis analysis [19].

The optimum synthesis of biological nanoparticles was achieved when the biomass used was 5 mg/mL. A temperature of 100 °C for 5 min resulted in the maximum yield of TiO₂NP. Further optimization of reaction temperature revealed that 40 °C was the optimal temperature for synthesis. Maximum absorbance was obtained for the biosynthesis of TiO₂NP when the salt concentration was 0.1 mM. The pH of the reaction was found to be a critical factor, with the best results obtained at a pH of 7.0. The optimum time for completing the synthesis process was 24 h, as per UV analysis (Figure 1a–g). The optimal extract-to-salt solution ratio for the bio-fabrication of TiO₂NP using Phormidium species was found to be 9:1.

Other researchers have reported different optimized reaction parameters using various biological sources for extract preparation. Roopan et al. (2013) found the optimal reaction temperature and time for phyto-synthesis of TiO₂NP using *Annona squamosa* peel extract to be 60 °C for 6 h [20]. The optimum conditions reported by Siddiqui et al. (2022) for the synthesis of TiO₂NP using *Synechocystis* NCCU-370 were pH 7.0, time 12 h, and temperature 30 °C [21].

After optimizing the extract and reaction conditions, cyanobacteria-mediated TiO₂NP was characterized via TEM, SEM, and XRD to evaluate the significant physicochemical properties. Careful analysis of the XRD pattern revealed the most substantial peak at 25.12° corresponding to 101, which confirmed the synthesis of anatase TiO₂NP (Figure 2A). The average size of the crystallite nanoparticles via XRD analysis was found to be 10.61 nm. The average size of the crystallite nanoparticles, calculated using the Debye–Scherrer equation, was 10.61 nm [22]. TEM analysis showed that the biosynthesized TiO₂NP existed as single crystals with spherical morphology and good dispersion (Figure 2B). This is similar to the size (16 nm) reported for TiO₂NP fabricated using a different strain of cyanobacteria [21]. Other studies have reported larger particle sizes for nanoparticles synthesized using non-cyanobacteria sources. Kumar et al. (2023) synthesized TiO₂NP using alpha-amylase and obtained an average grain size of 50 nm [23]. SEM micrographs also confirmed that the biosynthesized nanoparticles were spherical (Figure 2C).

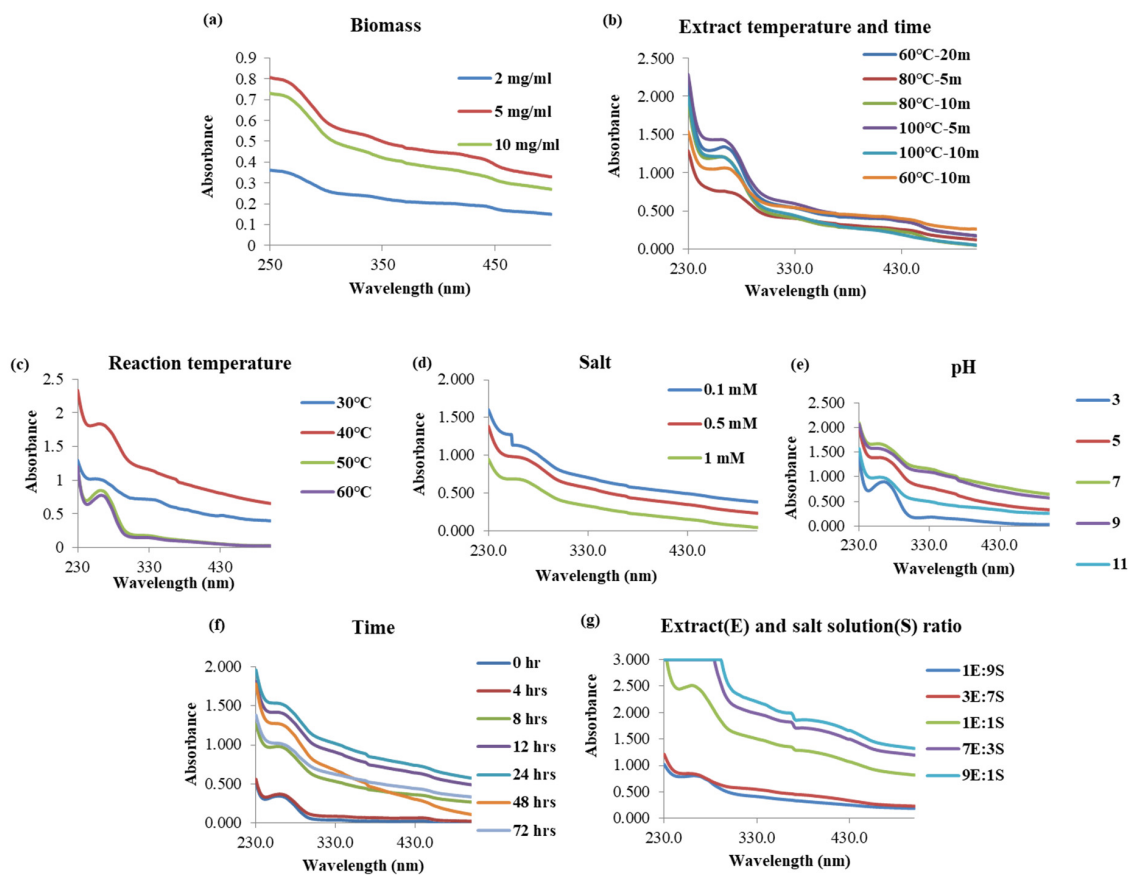


Figure 1. (a–g) shows the optimization of extract and reaction parameters.

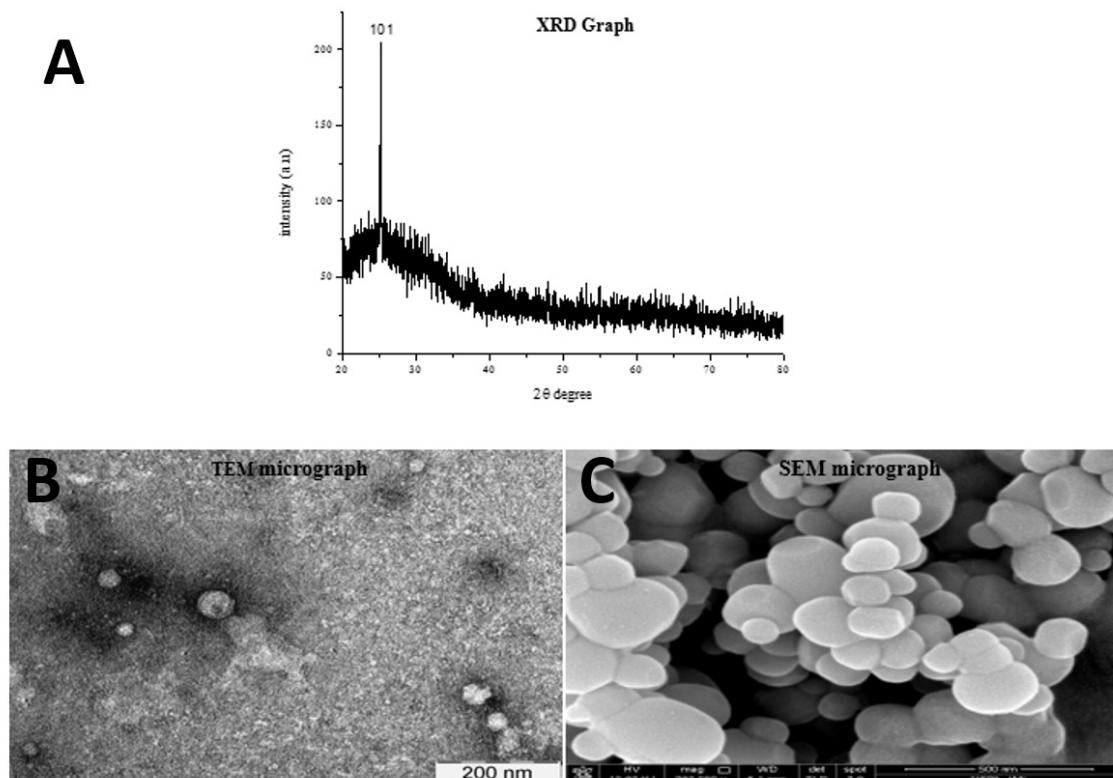


Figure 2. Characterization of TiO_2NP : (A) XRD; (B) TEM; (C) SEM.

2.2. Cyclic Voltammetry of Cathode

The CV experiment was performed to evaluate the ORR efficacy of the TiO₂ NP-loaded graphite sheet electrode. Graphite sheet coated with TiO₂NP as a working, counter, and reference electrode, the Ag/AgCl electrode, and Pt wire were utilized. The electrodes were inserted in a 1 M KCl electrolyte saturated with either O₂ or N₂ [24]. The scanning rate was set to 10 mV/s with a potential window from −0.6 V to 0.3 V (Figure 3). With 2.0 mg/cm² NP, a noticeable (near −0.1 V) peak appeared; however, 2 mg/cm² NPs did not produce a discernible reduction peak with an N₂-saturated KCl electrolyte. This might be due to the action of nanoparticles on the cathode surface that enhances electron transfer during ORR in the presence of oxygen. No peak was found in the unmodified graphite sheet.

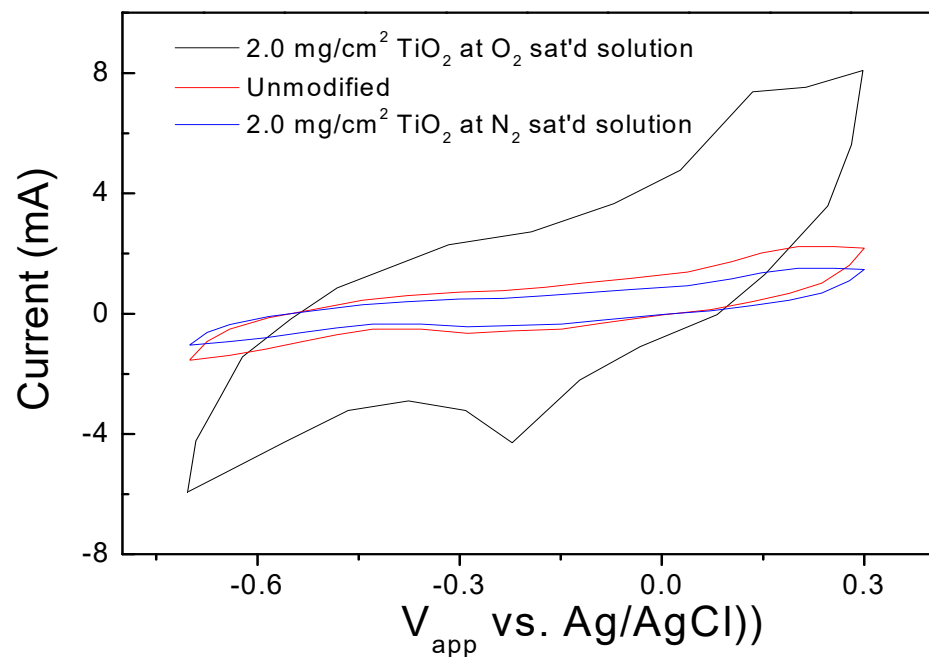


Figure 3. The effects of TiO₂ concentration at the cathode were measured using cyclic voltammetry at a scan rate of 2 mV/s.

These results indicate the effectiveness of TiO₂NP in enhancing ORR on the graphite electrode surface. Further optimization of TiO₂NP quantity was carried out to achieve maximum power output.

2.3. Polarization Study in MFC

During the solid-state MFC (MFC) test, each batch cycle lasted 36 h (± 2 h). Synthetic acetate-containing wastewater was delivered directly into the anodic chamber for 24 h without any inoculum. With a correction tolerance of 0.1, the effluent pH was maintained at a steady-state condition of 7.0. In the absence of inoculum, the anodic half-cell potential relative to the Ag/AgCl reference electrode was 192.07 mV, and no current was measured. These results suggest no biotic response occurring in the anode chamber. The anode chamber was then inoculated with anaerobic consortia recovered from the bottom sludge. After the adaptation period, the MFC was run in a fed-batch mode with a closed-circuit configuration at an ambient temperature of 37 °C. Following inoculation, the anodic half-cell potential began to decrease due to electron transfer from anodophiles until it hit a plateau of roughly −256 mV (vs. Ag/AgCl) vs. resistance of 100 Ω [25]. After four cycles, the anodic half-performance cell performance was found to be steady.

The cathodic half-cell potential was measured using composite electrodes prepared in this study, with the anodic potential stabilized [26]. The impact of loading TiO₂NPs onto carbon on power generation in an MFC was evaluated by incorporating different

concentrations (mg/cm^2) of TiO_2 NPs into Vulcan XC. It was found that the cathodic half-cell potential varied significantly depending on the amount of catalyst (TiO_2 -NPs) loading in the air cathode.

In an MFC, the polarization curve calculates the maximum volumetric power density (Pd_{max}) (Figure 4a). Different concentrations of TiO_2 NPs (0.5, 1.0, 1.5, 2.0, and 2.5 mg/cm^2) impregnated on graphite sheet cathode were used to study the impact of the TiO_2 NP on the power output in MFC. The cathode half-cell potential was found to vary significantly with changes in the amount of TiO_2 NP present in the cathode (Figure 4b). The maximum Pd_{max} of the cathode impregnated with 2.0 mg/cm^2 TiO_2 NP was 15.2 W/m^3 . In contrast, the Pd_{max} dramatically increased to 5.0, 7.4, 12.7, and 15 W/m^3 , respectively, with various concentrations 0.5, 1.0, 1.5, and 2.5 mg/cm^2 of TiO_2 NP on the cathode. When the nanoparticle concentration was increased from 0.5 to 1.0 mg/cm^2 , the Pd_{max} amplitude increased almost twice. However, the nanoparticle concentration difference between 2.0 and 2.5 mg/cm^2 only resulted in a 2.3% decrease in Pd_{max} . As the concentration of nanoparticles increased, the COD removal efficiency and the maximum Coulombic efficiency (CE) also increased, with a peak at 2.5 mg/cm^2 of TiO_2 NP on the cathode. The internal resistance decreased as the concentration of nanoparticles increased, as shown in Figure 5. This indicates that the addition of nanoparticles to the cathode significantly improved the MFC's ability to generate electricity.

2.4. Electrochemical Impedance Studies

The semicircle area of the cathode's impedance plot exhibits a significant change, as shown in Figure 5 [27]. The observations are made using the Nyquist or Bode plot techniques, which evaluate both the "imaginary" and "actual" impedances. The accompanying graph displays the impedance against frequency, with the X-axis showing the impedance vs. frequency and the Y-axis showing the phase angle and specific impedance value. The highest resistance is found at the point of the highest frequency. When 2.0 mg/cm^2 of TiO_2 NP is present on the cathode of a microbial fuel cell (MFC), the lowest R_{ct} value indicates the greatest electron transport due to high substrate degradation. This leads to improved current generation and increased anodic voltage losses. The conclusions of the EIS align with those of the half-cell polarization research. Based on the R_{ct} values, MFC cathodes with nanoparticle (NP) concentrations of 1.0 mg/cm^2 (35.6 Ω), 1.5 mg/cm^2 (38.5 Ω), and 2.0 mg/cm^2 (9.2 Ω) were analyzed and showed respective internal resistances. The decreased internal resistance with TiO_2 NP loading is attributed to increased oxygen reduction kinetics at the cathode surface.

2.5. COD Elimination and Coulombic Efficiency

The batch operation of the MFC was regularly monitored for COD removal and Coulombic efficiency (CE) (Figure 6). After 25 batch cycles (38 days), MFC with a cathode containing 2.0 mg/cm^2 of TiO_2 NPs showed up to 87.8% COD removal with a CE of 8.68. The results indicate that 2.0 mg/cm^2 of TiO_2 NPs is the optimal concentration for maximum power output and CE, as no significant difference was observed with higher catalyst concentrations. The CE was 38.5% lower in MFC with 0.5 mg/cm^2 NPs TiO_2 NP. This result suggested cathode catalyst plays a vital role in electrochemical wastewater treatment.

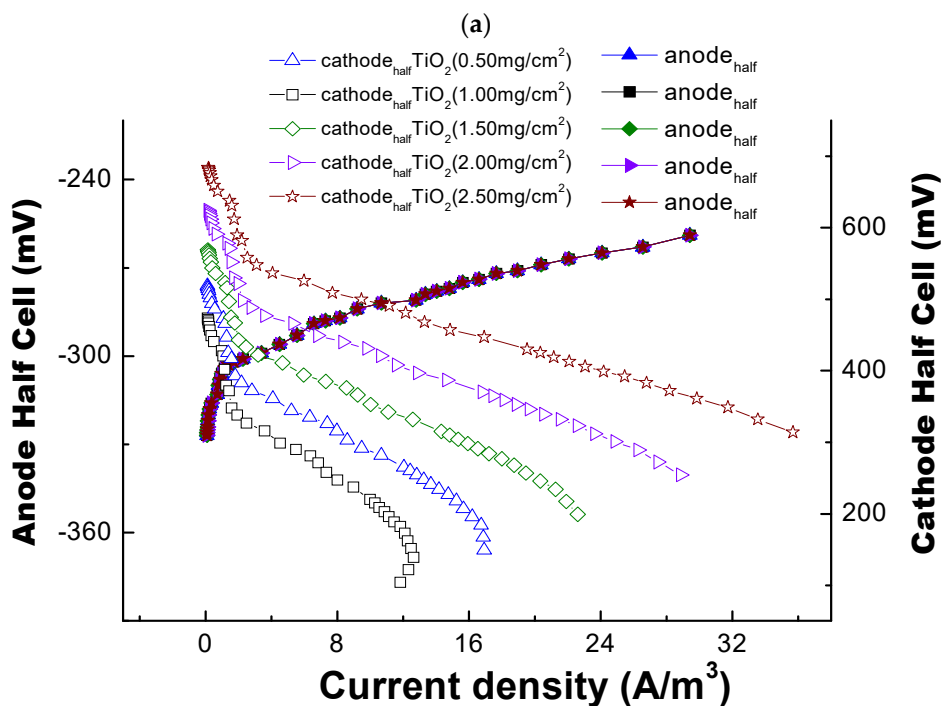
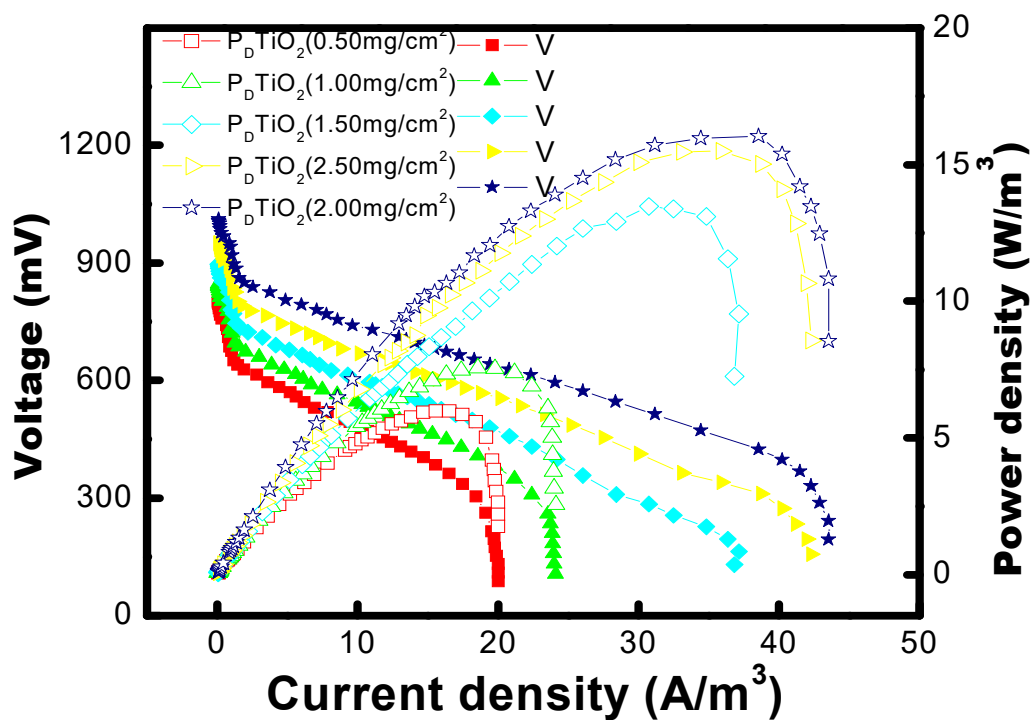


Figure 4. (a) Polarization plots with varying nanoparticles for MFCs (power density and DC voltage as a function of current density). Voltage points and volumetric power density data are displayed as open and solid symbols, respectively. (b) Analysis of the volumetric current density of anode and cathode half-cells. The anode and cathode half-cell voltage data points are represented by solid and open symbols.

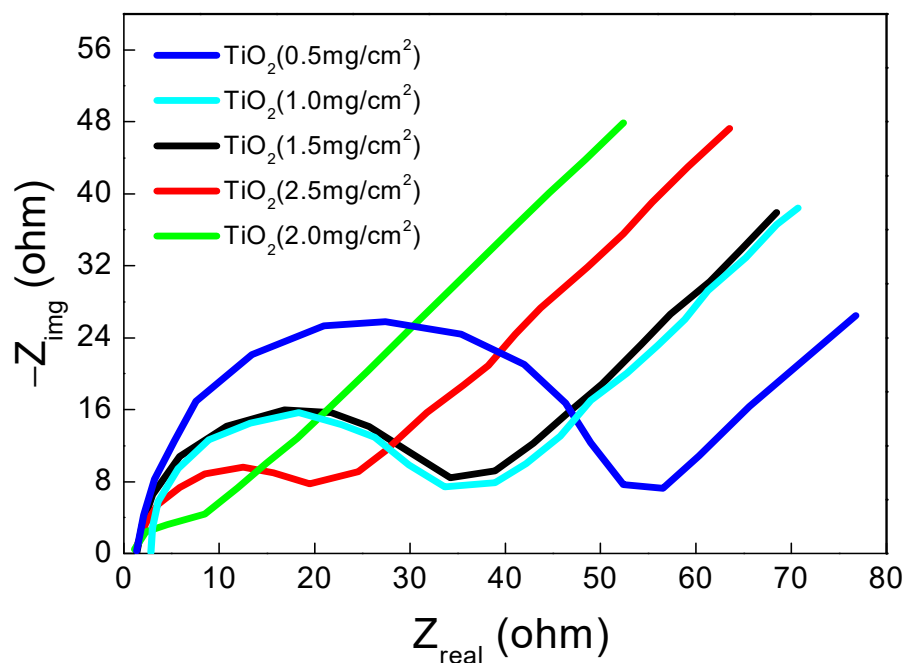


Figure 5. MFCs loaded with 0.5, 1, 1.5, 2, and 2.5 mg/cm² of TiO₂ were observed on a 1 MHz to 100 kHz Nyquist plot (WE = working electrode; R_s = solution resistance; CPE = constant phase element; R_{ct} = charge transfer resistance; W = Warburg element; CE = counter electrode).

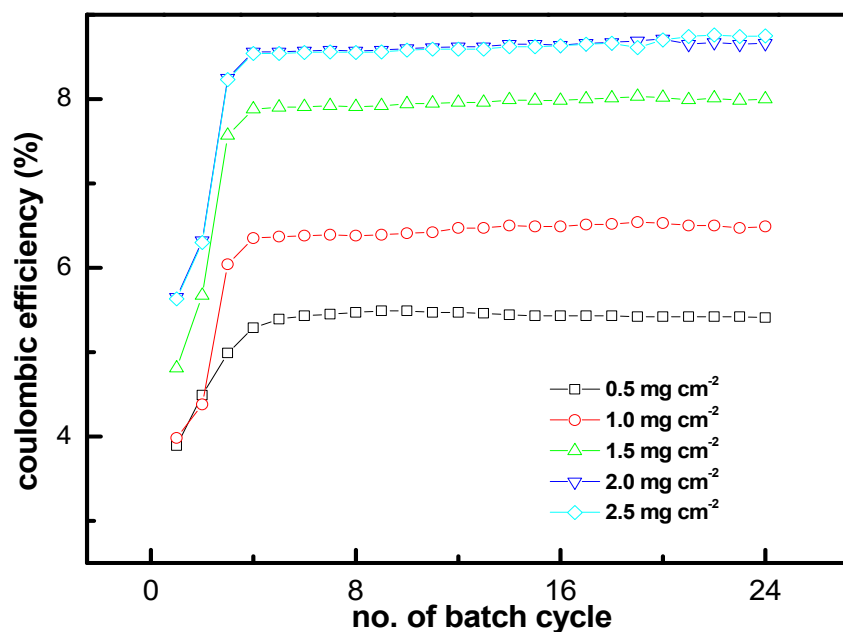


Figure 6. Coulombic efficiency measured in %, after experimentation with several concentrations of the nanoparticle-loaded cathode.

2.6. Biofouling Studies on the Cathode Surface

According to the CSLM data, the cathode loading 2.0 mg/cm² had fewer microbial cells than the cathode without TiO₂. The results revealed that the cathode's less hazardous surface caused the highest number of cells on graphite electrodes without TiO₂. TiO₂ was added to the cathode to boost its toxicity, preventing undesirable biofilm development. This study has shown that the performance of the MFC with the maximum power density produced by TiO₂ of loading 2.0 mg/cm² increased significantly as the TiO₂ concentration

was increased from 0.5 mg/cm² to 2.0 mg/cm². The IMARIS images supported the findings (Figure 7).

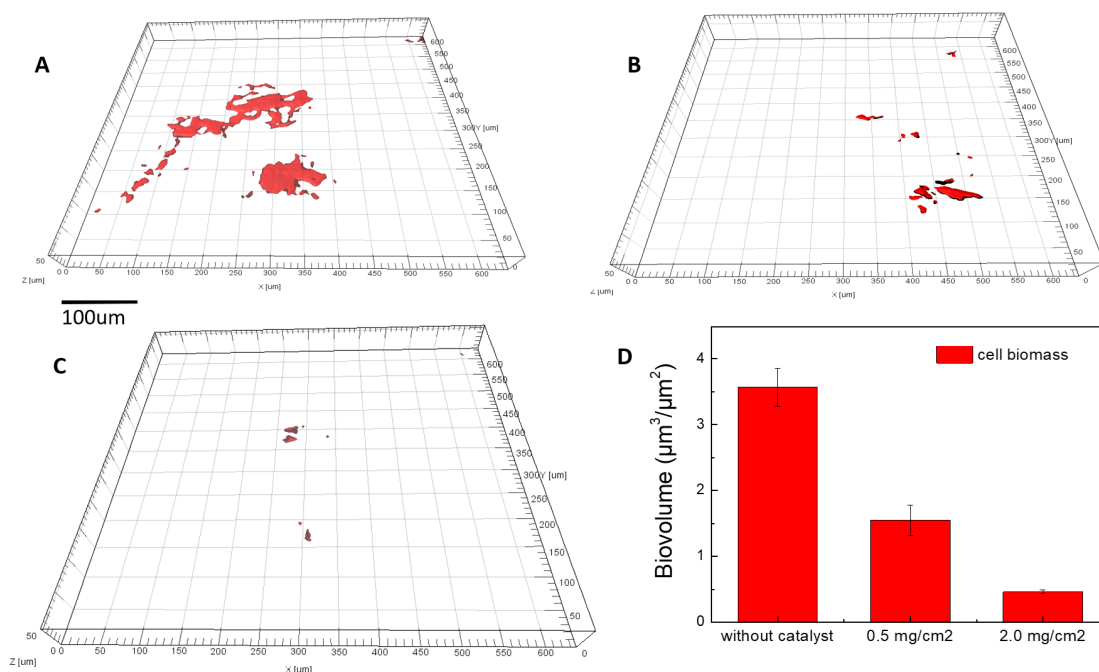


Figure 7. IMARIS 3-D photos of biofilms on various TiO₂ concentrations with graphite cathode: (A) pristine graphite sheet; (B) graphite impregnated with 0.5 mg/cm² TiO₂; (C) graphite cathode impregnated with 2.0 mg/cm² TiO₂. The red clusters represent microbial cell biomass on a graphite cathode containing TiO₂. (D) The biovolume of biofouling on the various cathode surfaces.

3. Materials and Method

3.1. Fabrication of an Impregnated Graphite Sheet Cathode Using Synthesized Biogenic TiO₂ Nanoparticle

According to previous research, the biosynthesis of TiO₂ nanoparticles (NPs) was performed using the Phormidium species NCCU-104 cyanobacterium [21]. The process involved the preparation of an aqueous extract of the dried cyanobacterial biomass. The biomass was mixed with double distilled water, homogenized, and sonicated for 3 min. The mixture was then subjected to a water bath for a few minutes, followed by centrifugation and filtration using Whatman filter paper [28]. The resulting supernatant was then used as the extract and reacted with titanium salt to synthesize the NPs. To optimize the biosynthesized NPs, specific reaction parameters were selected. The optimization of the extract preparation process was carried out by varying the biomass concentration (2, 5, and 10 mg/mL), temperature (60, 80, and 100 °C), and time (5, 10, and 20 min) during the preparation of the extract.

Optimization of extract conditions was followed by optimization of reaction parameters such as temperature, salt concentration, pH, time, and salt-to-extract ratio. To investigate the impact of temperature on the creation of TiO₂ NPs, the temperature range involved (30, 40, 50, and 60 °C) was utilized while maintaining consistency in other reaction parameters. Similarly, the reaction was carried out at different salt concentrations (0.1, 1, 0.5, and 1 mM). Moreover, to understand more about how pH affects the creation of TiO₂ nanoparticles, a range of pH values (3, 5, 7, 9, and 11) were tested. The synthesis was monitored from 0 to 72 h at regular intervals. Lastly, to find the optimal ratio, the reaction was also run at various extract-to-salt ratios (1:9, 3:7, 1:1, 7:3, and 9:1).

3.2. Characterization of Cyanobacteria-Derived TiO₂ NPs

Transmission electron microscopy (TEM), high-resolution field emission scanning electron microscopy (HR-FESEM), and X-ray diffraction (XRD) were used to examine cyanobacteria-derived TiO₂ nanoparticles and determine their physicochemical parameters [21]. The purified nanoparticles were dissolved in ethanol, sonicated, and filtered prior to analysis. The TEM analysis was performed using a Tecnai G2 Spirit, BioTWIN New York, NY, USA, 10031 device subjected to a voltage of 120 kV accelerating. The sample was then treated with a 1% solution of uranyl acetate for 1 h (Siddiqui et al., 2022a). The NPs were then placed on a carbon-coated copper grid for analysis. HR-FESEM analysis was performed by placing nanoparticles on clean and dry glass slides. Then, the nanoparticles were coated with gold. The images were captured using the voltage accelerated at 20 kV using Nova NanoSEM 650 SEM. The XRD pattern of the Phormidium-mediated TiO₂NP was obtained using XRD Rigaku Ultima IV, Austin, TX, USA. The XRD was performed in the range of 20° to 80° at a voltage of 40 kV [21].

The nanoparticles were dissolved in 50 mL of deionized water using a titanium horn edge sonicator (Piezo-U-Sonic, Delhi, India). The composite mixture was formed after adding 0.5 mL of Nafion solution and sonicating it for 30 min. The functional contact area was roughly 9 cm² (3.0 cm × 3.0 cm), and the graphite sheet was cleaned with 1 M HCl to eliminate debris or dust [21]. After 30 min of sonication in distilled water to remove any lingering debris, the components were extensively cleaned in a 35% ethanol/distilled water solution. The sonicated nanoparticles were then blended with Nafion solution and sprayed at varying concentrations over the graphite sheet to create the nanoparticle-modified cathode, which was stored overnight at 60 °C [29].

3.3. MFC Construction

For the studies, six identical MFCs were developed. For the studies, six identical MFCs were developed. The anode consisted of a graphite felt and a 300 mL-capacity earthenware chamber with exterior dimensions of 7 × 8 × 3.5 cm³ were used to fabricate microbial fuel cell. The membrane cathode assembly (MCA) was situated on the opposite side of the MFC from the anode. The anode chamber was equipped with two ports on the top; one served as a reference electrode and sampling (saturated KCl; +197 mV, Equiptronics, Ag/AgCl, Mumbai, India), while the other served as the electrode terminal. 18 cm² carbon felt served as the cathode, and a stainless steel wire was connected to it [30]. The MCA was made by covering the membrane with a different concentration of biogenic TiO₂-NP (0.5–2.5 mg/cm²) with 3 mg/cm² of a fixed concentration of Vulcan XC-72 [31]. Out of six MFCs, one MFC was undoped as a control. The cathode terminal was connected to concealed copper wires, and the wires completed the circuit by connecting to the external resistance. The anodes in each experiment were placed at the same distance from the MCA, and the inter-electrode spacing was maintained at 2.5 cm. The additional ports were plugged with clapped tubes to establish an anaerobic environment. Before the experiment, the MFCs were left for 30 min in the UV chamber and cleaned using 70% alcohol.

3.4. Anodic Mixed Consortia and Anolyte

As the parent inoculum, a neutral pH bottom sludge was obtained from a local septic tank to establish an anaerobic complex microbial consortium. The sludge was pre-treated to 105 °C for 15 min [32]. Anode inoculum was prepared from the pre-treated sludge, sieved through a 1 mm mesh, and bioaugmented with a locally isolated electroactive bacteria, *Pseudomonas aeruginosa* SU-B2 [33]. In order to assess bacterial growth, 10 mL aliquots of culture were obtained at different time intervals for which their cell densities were measured using a SHIMADZU UV/Visible spectrophotometer at 600 nm. Bacterial cells were pelleted after centrifugation at 15,000 rpm for 20 min, and the supernatant was separated to detect the concentration of a specific color using a spectrophotometer. The anolyte was prepared using an acetate medium with a COD of 3000 mg/L and was adjusted to the desired pH with a low-strength acidic or basic solution. The MFCs were

operated in batch mode with 36 h repetition cycles at around 37 °C. The initial anolyte pH was optimized by changing the pre-treated inoculum and adjusting the pH with acidic or basic solutions.

3.5. Performance Evaluation of MFCs

In order to evaluate the performance of the MFCs, various measurements were performed. The chemical oxygen demand (COD) of the anolyte was determined using COD measuring instruments (TopLab Pvt. Ltd., Mumbai, India) [34]. A Potentiostat was used to measure the voltage potential of the MFCs (Biologic SP-150, India). The MFCs were operated in open circuit mode to allow them to achieve their maximum voltage, which resulted in polarisation curves [35]. The closed circuit's external resistance was adjusted in periodic increments with a variable resistance box (range 90 K–20 K) to measure the resulting voltage drop, producing polarisation curves. Coulombic efficiency, volumetric power density, and current density were calculated based on the results of these measurements. A three-electrode setup was used to perform electrochemical tests, with the cathode as the working electrode, Pt wire as the counter electrode, and Ag/AgCl serving as the reference electrode [36]. With a scan rate of 2 mV/s, cyclic voltammetry (CV) was carried out in the potential range of -0.6 to $+0.3$ V. Additionally, a new electrode design was used for electrochemical impedance spectroscopy (EIS), using a Pt wire as the reference electrode, the anode as the working electrode, and the cathode as the counter electrode. A 5 mV sinusoidal disturbance with a 100 kHz to 1 Hz frequency range was used to perform the EIS [31].

3.6. Biofouling Studies on TiO₂-Impregnated Cathode Surface

MFCs cathode with various concentration of TiO₂-coated was evaluated. Two cathodes were used: graphite sheet used as a control against the TiO₂-impregnated graphite at 2.0 mg/cm² loading rates. Each cathode type's average biovolume of cell biomass was calculated and displayed for evaluation [37]. The biofilm stain solution was made using a phosphate-buffered saline (PBS) solution containing 3 μM propidium iodide. The different cathodes were carefully removed after biofouling on the MFC cathode and cut into approximately 5 mm × 5 mm pieces. The biofouling was stained after being incubated in the stain solution for 30 min in the dark. We used a confocal laser scanning microscope (CLSM; ZeissMeta510; Carl ZEISS, Inc., White Plains, NY, USA) equipped with a Zeiss dry objective LCI to examine the stained biofouling samples [35]. Plan-Neo Fluor (0.5 numerical aperture, 20× magnification). Ten different locations on each surface were used to stack photos stitched together. COMSTAT, an image processing program, was used for the image analysis in order to determine the precise biovolume (μm³/μm²) in the biofouling layer. It was created as a script and combined with an image processing toolkit in Matlab 6.5 (The Math Works, Inc., Natick, MA, USA). Every sample had 10 places on each graphite electrode chosen for microscopical observation and analysis. Using the Imaris application, the CLSM image stacks were recreated in three dimensions (Imaris Bitplane, Zurich, Switzerland). The average biovolume of cells was measured for various kinds and concentrations of graphite electrodes containing TiO₂ [32].

4. Conclusions

In order to enhance the performance of MFCs, biogenic TiO₂ nanoparticles (NPs) were utilized as a catalyst. These NPs have a nano-porous morphology that improves electrode/electrolyte interaction and substrate dispersion to the electrode. Additionally, biogenic TiO₂NPs have a high specific area, biocompatibility, conductivity, and chemical stability, making them an attractive option for MFC cathode catalysts. The best results were achieved using carbon felt impregnated with TiO₂NPs, which showed long-term durability and high power production. An optimized concentration of 2.0 mg/cm² was found to have the highest catalytic activity, power output, and stability. The TiO₂NP-impregnated cathode also has selective antibacterial properties, affecting the composition of the bacterial

population on the cathode and contributing to the MFC's long-term stability and good performance. This work provides insight into the relationship between the catalyst and microbial population and offers a potential approach for creating a bifunctional cathodic catalyst in MFCs.

Author Contributions: Conceptualization, S.P.; methodology, A.K., T.S., A.R. and T.F.; formal analysis, A.G. and A.A.S.; investigation, A.S.M. and S.R.; resources, P.S. and K.K.Y.; writing—original draft preparation, A.K., T.S., S.P., A.R. and T.F.; writing—review and editing, H.-K.P. and B.-H.J.; funding acquisition, H.-K.P. and B.-H.J. All authors have read and agreed to the published version of the manuscript.

Funding: This project was supported by Researchers Supporting Project number (RSP2023R238), King Saud University, Riyadh, Saudi Arabia. This work was supported by the Mid-Career Researcher Program (grant no. 2020R1A2C3004237) through the National Research Foundation of the Republic of Korea.

Data Availability Statement: Not applicable.

Conflicts of Interest: The authors declare no conflict of interest.

References

1. Obileke, K.; Onyeaka, H.; Meyer, E.L.; Nwokolo, N. Microbial Fuel Cells, a Renewable Energy Technology for Bio-Electricity Generation: A Mini-Review. *Electrochem. Commun.* **2021**, *125*, 107003. [[CrossRef](#)]
2. Kurniawan, T.A.; Othman, M.H.D.; Liang, X.; Ayub, M.; Goh, H.H.; Kusworo, T.D.; Mohyuddin, A.; Chew, K.W. Microbial Fuel Cells (MFC): A Potential Game-Changer in Renewable Energy Development. *Sustainability* **2022**, *14*, 16847. [[CrossRef](#)]
3. Tsekouras, G.J.; Deligianni, P.M.; Kanellos, F.D.; Kontargyri, V.T.; Kontaxis, P.A.; Manousakis, N.M.; Elias, C.N. Microbial Fuel Cell for Wastewater Treatment as Power Plant in Smart Grids: Utopia or Reality? *Front. Energy Res.* **2022**, *10*, 370. [[CrossRef](#)]
4. Flimban, S.G.A.; Ismail, I.M.I.; Kim, T.; Oh, S.-E. Overview of Recent Advancements in the Microbial Fuel Cell from Fundamentals to Applications: Design, Major Elements, and Scalability. *Energies* **2019**, *12*, 3390. [[CrossRef](#)]
5. Mecheri, B.; Gokhale, R.; Santoro, C.; Costa de Oliveira, M.A.; D'Epifanio, A.; Licocchia, S.; Serov, A.; Artyushkova, K.; Atanassov, P. Oxygen Reduction Reaction Electrocatalysts Derived from Iron Salt and Benzimidazole and Aminobenzimidazole Precursors and Their Application in Microbial Fuel Cell Cathodes. *ACS Appl. Energy Mater* **2018**, *1*, 5755–5765. [[CrossRef](#)]
6. Jiang, M.; Yu, X.; Yang, H.; Chen, S. Optimization Strategies of Preparation of Biomass-Derived Carbon Electrocatalyst for Boosting Oxygen Reduction Reaction: A Minireview. *Catalysts* **2020**, *10*, 1472. [[CrossRef](#)]
7. Costa de Oliveira, M.A.; D'Epifanio, A.; Ohnuki, H.; Mecheri, B. Platinum Group Metal-Free Catalysts for Oxygen Reduction Reaction: Applications in Microbial Fuel Cells. *Catalysts* **2020**, *10*, 475. [[CrossRef](#)]
8. Yin, J.; Wei, K.; Bai, Y.; Liu, Y.; Zhang, Q.; Wang, J.; Qin, Z.; Jiao, T. Integration of Amorphous CoSnO₃ onto Wrinkled MXene Nanosheets as Efficient Electrocatalysts for Alkaline Hydrogen Evolution. *Sep. Purif. Technol.* **2023**, *308*, 122947. [[CrossRef](#)]
9. Yin, J.; Zhan, F.; Jiao, T.; Deng, H.; Zou, G.; Bai, Z.; Zhang, Q.; Peng, Q. Highly Efficient Catalytic Performances of Nitro Compounds via Hierarchical PdNPs-Loaded MXene/Polymer Nanocomposites Synthesized through Electrospinning Strategy for Wastewater Treatment. *Chin. Chem. Lett.* **2020**, *31*, 992–995. [[CrossRef](#)]
10. Yin, J.; Zhan, F.; Jiao, T.; Wang, W.; Zhang, G.; Jiao, J.; Jiang, G.; Zhang, Q.; Gu, J.; Peng, Q. Facile Preparation of Self-Assembled MXene@Au@CdS Nanocomposite with Enhanced Photocatalytic Hydrogen Production Activity. *Sci. China Mater.* **2020**, *63*, 2228–2238. [[CrossRef](#)]
11. Xu, X.; Wang, W.; Zhou, W.; Shao, Z. Recent Advances in Novel Nanostructuring Methods of Perovskite Electrocatalysts for Energy-Related Applications. *Small Methods* **2018**, *2*, 1800071. [[CrossRef](#)]
12. Zhang, X.; Xu, X.; Yao, S.; Hao, C.; Pan, C.; Xiang, X.; Tian, Z.; Shen, P.; Shao, Z.; Jiang, S. Boosting Electrocatalytic Activity of Single Atom Catalysts Supported on Nitrogen-Doped Carbon through N Coordination Environment Engineering. *Small* **2022**, *18*, 2105329. [[CrossRef](#)] [[PubMed](#)]
13. Quinn, J.; McFadden, R.; Chan, C.-W.; Carson, L. Titanium for Orthopedic Applications: An Overview of Surface Modification to Improve Biocompatibility and Prevent Bacterial Biofilm Formation. *iScience* **2020**, *23*, 101745. [[CrossRef](#)] [[PubMed](#)]
14. Ajsuvakova, O.P.; Tinkov, A.A.; Aschner, M.; Rocha, J.B.T.; Michalke, B.; Skalnaya, M.G.; Skalny, A.V.; Butnariu, M.; Dadar, M.; Sarac, I.; et al. Sulfhydryl Groups as Targets of Mercury Toxicity. *Coord Chem. Rev.* **2020**, *417*, 213343. [[CrossRef](#)] [[PubMed](#)]
15. Suresh, S.; Imteyaz, S.; Murugan, B.; Lett, A.; Sridewi, N.; Kassegn, G.; Fatimah, I.; Oh, W.-C. A Comprehensive Review on Green Synthesis of Titanium Dioxide Nanoparticles and Their Diverse Biomedical Applications. *Green Process. Synth.* **2022**, *11*, 44–63. [[CrossRef](#)]
16. Ziental, D.; Czarczynska-Goslinska, B.; Mlynarczyk, D.T.; Glowacka-Sobotta, A.; Stanisz, B.; Goslinski, T.; Sobotta, L. Titanium Dioxide Nanoparticles: Prospects and Applications in Medicine. *Nanomaterials* **2020**, *10*, 387. [[CrossRef](#)]
17. Pei, D.-N.; Gong, L.; Zhang, A.-Y.; Zhang, X.; Chen, J.-J.; Mu, Y.; Yu, H.-Q. Defective Titanium Dioxide Single Crystals Exposed by High-Energy {001} Facets for Efficient Oxygen Reduction. *Nat. Commun.* **2015**, *6*, 8696. [[CrossRef](#)]

18. Santhoshkumar, T.; Rahuman, A.A.; Jayaseelan, C.; Rajakumar, G.; Marimuthu, S.; Kirthi, A.V.; Velayutham, K.; Thomas, J.; Venkatesan, J.; Kim, S.-K. Green Synthesis of Titanium Dioxide Nanoparticles Using Psidium Guajava Extract and Its Antibacterial and Antioxidant Properties. *Asian Pac. J. Trop. Med.* **2014**, *7*, 968–976. [[CrossRef](#)] [[PubMed](#)]
19. Mughal, B.; Zaidi, S.Z.J.; Zhang, X.; Hassan, S.U. Biogenic Nanoparticles: Synthesis, Characterisation and Applications. *Appl. Sci.* **2021**, *11*, 2598. [[CrossRef](#)]
20. Roopan, S.M.; Rohit; Madhumitha, G.; Rahuman, A.A.; Kamaraj, C.; Bharathi, A.; Surendra, T.V. Low-Cost and Eco-Friendly Phyto-Synthesis of Silver Nanoparticles Using Cocos Nucifera Coir Extract and Its Larvicidal Activity. *Ind. Crops Prod.* **2013**, *43*, 631–635. [[CrossRef](#)]
21. Siddiqui, T.; Khan, N.J.; Asif, N.; Ahamad, I.; Yasin, D.; Fatma, T. Screening, Characterisation and Bioactivities of Green Fabricated TiO₂ NP via Cyanobacterial Extract. *Environ. Sci. Pollut. Res. Int.* **2022**, *29*, 39052–39066. [[CrossRef](#)]
22. Siddiqui, T.; Khan, N.J.; Fatma, T. Green Synthesis of Titanium Dioxide Nanoparticles and Their Applications. In *Sustainable Nanotechnology*; John Wiley & Sons, Ltd.: Hoboken, NJ, USA, 2022; pp. 135–142, ISBN 978-1-119-65029-4.
23. Kumar, A.; Sharma, K.; Pandit, S.; Singh, A.; Prasad, R. Evaluation of the Algal-Derived Biochar as an Anode Modifier in Microbial Fuel Cells. *Bioresour. Technol. Rep.* **2023**, *22*, 101414. [[CrossRef](#)]
24. Khilari, S.; Pandit, S.; Das, D.; Pradhan, D. Manganese Cobaltite/Polypyrrole Nanocomposite-Based Air-Cathode for Sustainable Power Generation in the Single-Chambered Microbial Fuel Cells. *Biosens. Bioelectron.* **2014**, *54*, 534–540. [[CrossRef](#)]
25. Khilari, S.; Pandit, S.; Ghangrekar, M.M.; Das, D.; Pradhan, D. Graphene Supported α -MnO₂ Nanotubes as a Cathode Catalyst for Improved Power Generation and Wastewater Treatment in Single-Chambered Microbial Fuel Cells. *RSC Adv.* **2013**, *3*, 7902–7911. [[CrossRef](#)]
26. Chauhan, S.; Kumar, A.; Pandit, S.; Vempaty, A.; Kumar, M.; Thapa, B.S.; Rai, N.; Peera, G. Investigating the Performance of a Zinc Oxide Impregnated Polyvinyl Alcohol-Based Low-Cost Cation Exchange Membrane in Microbial Fuel Cells. *Membranes* **2023**, *13*, 55. [[CrossRef](#)] [[PubMed](#)]
27. Pandit, S.; Khilari, S.; Roy, S.; Pradhan, D.; Das, D. Improvement of Power Generation Using Shewanella Putrefaciens Mediated Bioanode in a Single Chambered Microbial Fuel Cell: Effect of Different Anodic Operating Conditions. *Bioresour. Technol.* **2014**, *166*, 451–457. [[CrossRef](#)]
28. Sharma, K.; Pandit, S.; Thapa, B.S.; Pant, M. Biodegradation of Congo Red Using Co-Culture Anode Inoculum in a Microbial Fuel Cell. *Catalysts* **2022**, *12*, 1219. [[CrossRef](#)]
29. Sharma, K.; Singh, V.; Pandit, S.; Thapa, B.S.; Pant, K.; Tusher, T. Isolation of Biosurfactant-Producing Bacteria and Their Co-Culture Application in Microbial Fuel Cell for Simultaneous Hydrocarbon Degradation and Power Generation. *Sustainability* **2022**, *14*, 15638. [[CrossRef](#)]
30. Kishimoto, N.; Okumura, M. Feasibility of Mercury-Free Chemical Oxygen Demand (COD) Test with Excessive Addition of Silver Sulfate. *J. Water Environ. Technol.* **2018**, *16*, 221–232. [[CrossRef](#)]
31. Vempaty, A.; Kumar, A.; Pandit, S.; Gupta, M.; Mathuriya, A.S.; Lahiri, D.; Nag, M.; Kumar, Y.; Joshi, S.; Kumar, N. Evaluation of the Datura Peels Derived Biochar-Based Anode for Enhancing Power Output in Microbial Fuel Cell Application. *Biocatal. Agric. Biotechnol.* **2023**, *47*, 102560. [[CrossRef](#)]
32. Sharma, K.; Pandit, S.; Singh, A.; Gupta, P.; Pant, K. Microbial Electrochemical Treatment of Methyl Red Dye Degradation Using Co-Culture Method. *Water* **2023**, *15*, 56. [[CrossRef](#)]
33. Pandit, S.; Jadhav, D.; Singh, A.; Pandit, C. Blue Energy Meets Green Energy in Microbial Reverse Electrodialysis Cells: Recent Advancements and Prospective. *Sustain. Energy Technol. Assess.* **2023**, *57*, 103260. [[CrossRef](#)]
34. Arya, G.; Kumari, M.; Pundir, R.; Chatterjee, S.; Gupta, N.; Kumar, A.; Chandra, R.; Nimesh, S. Versatile Biomedical Potential of Biosynthesized Silver Nanoparticles from Acacia Nilotica Bark. *J. Appl. Biomed.* **2019**, *17*. [[CrossRef](#)] [[PubMed](#)]
35. Canchanya-Huaman, Y.; Mayta-Armas, A.F.; Pomalaya-Velasco, J.; Bendezú-Roca, Y.; Guerra, J.A.; Ramos-Guivar, J.A. Strain and Grain Size Determination of CeO₂ and TiO₂ Nanoparticles: Comparing Integral Breadth Methods versus Rietveld, μ -Raman, and TEM. *Nanomaterials* **2021**, *11*, 2311. [[CrossRef](#)] [[PubMed](#)]
36. Ahmad, R.; Mohsin, M.; Ahmad, T.; Sardar, M. Alpha Amylase Assisted Synthesis of TiO₂ Nanoparticles: Structural Characterization and Application as Antibacterial Agents. *J. Hazard. Mater.* **2015**, *283*, 171–177. [[CrossRef](#)]
37. Sun, Y.; ter Heijne, A.; Rijnaarts, H.; Chen, W.-S. The Effect of Anode Potential on Electrogenesis, Methanogenesis and Sulfidogenesis in a Simulated Sewer Condition. *Water Res.* **2022**, *226*, 119229. [[CrossRef](#)]

Disclaimer/Publisher's Note: The statements, opinions and data contained in all publications are solely those of the individual author(s) and contributor(s) and not of MDPI and/or the editor(s). MDPI and/or the editor(s) disclaim responsibility for any injury to people or property resulting from any ideas, methods, instructions or products referred to in the content.